BIOCHEMISTRY
including biophysical chemistry & molecular biology

Article

pubs.acs.org/biochemistry

Quaternary-Linked Changes in Structure and Dynamics That Modulate O_2 Migration within Hemoglobin's Gas Diffusion Tunnels

Maria S. Shadrina, Gilles H. Peslherbe,* and Ann M. English*

Department of Chemistry and Biochemistry, Centre for Research in Molecular Modeling and PROTEO, Concordia University, Montreal, Quebec H4B 1R6, Canada

Supporting Information

ABSTRACT: Atomistic molecular dynamics simulations of diffusion of O_2 from the hemes to the external solvent in the α- and β-subunits of the human hemoglobin (HbA) tetramer reveal transient gas tunnels that are not seen in crystal structures. We find here that the tunnel topology, which encompasses the reported experimental Xe binding cavities, is identical in HbA's T, R, and R2 quaternary states. However, the O_2 population in the cavities and the preferred O_2 escape portals vary significantly with quaternary structure. For example, most O_2 molecules escape from the T β-subunit via the cavity at the center of the tetramer, but direct exit from the distal heme pocket dominates in the R2 β-subunit. To understand what triggers the quaternary-linked redistribution of O_2 within its tunnels, we examined how the simulated tertiary structure and dynamics of each subunit differs among T, R, and R2 and report that minor adjustments in α-chain dynamics and β-heme position modulate O_2 distribution and escape in HbA. Coupled to the β-heme position, residue βF71 undergoes quaternary-linked conformations that strongly regulate O_2 migration between the β-subunit and HbA's central cavity. Remarkably, the distal histidine (HisE7) remains in a closed conformation near the α- and β-hemes in all states, but this does not prevent an average of 23, 31, and 46% of O_2 escapes from the distal heme pockets of T, R, and R2, respectively, via several distal portals, with the balance of escapes occurring via the interior tunnels. Furthermore, preventing or restricting the access of O_2 to selected cavities by mutating HisE7 and other heme pocket residues to tryptophan reveals how O_2 migration adjusts to the bulky indole ring and sheds light on the experimental ligand binding kinetics of these variants. Overall, our simulations underscore the high gas porosity of HbA in its T, R, and R2 quaternary states and provide new mechanistic insights into why undergoing transitions among these states likely ensures effective O_2 delivery by this tetrameric protein.

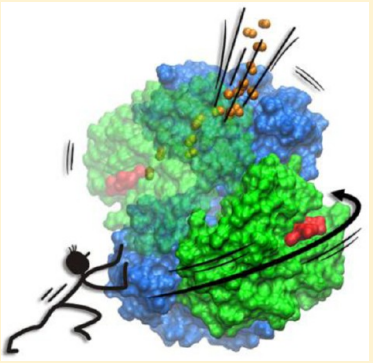

Comprised of two α-subunits and two β-subunits, the human hemoglobin tetramer (HbA) reversibly binds four O_2 ligands at its heme prosthetic groups. HbA undergoes a transition between well-characterized tense (T) and relaxed (R) quaternary states, which promotes positive cooperativity in ligand binding and ensures effective tissue oxygenation.[1] Crystal structures of the unligated T and fully ligated R states[2−5] have illuminated the structural changes accompanying the R−T transition, but despite a wealth of structural information about HbA's quaternary structures, little is known about how its quaternary transitions affect O_2 migration within the protein.

To explore the influence of quaternary structure on gas diffusion and escape in HbA, we compare the kinetically accessible O_2 diffusion tunnels in T and R by means of all-atom molecular dynamics (MD) simulations. An R2 quaternary structure also has been determined for ligated HbA,[6,7] and because it differs significantly from both R and T,[3−5] we additionally examine O_2 diffusion in R2. Experimental studies of heme pocket variants of HbA reveal that the point mutations in the distal heme pockets but not in the interior tunnels significantly influence ligand binding kinetics in HbA.[8−10] Thus, we probe the influence of mutation around the distal pocket on ligand migration by simulating O_2 diffusion in five variants with HisE7 and other residues mutated to a bulky tryptophan residue.

To facilitate studies of gas diffusion in a protein assembly such as HbA, we recently optimized atomistic MD simulations using temperature-controlled locally enhanced sampling (TLES)[11] and Langevin dynamics with a low damping coefficient (γ = 0.5 ps^{-1}).[12] Unlike implicit sampling and void-volume-search approaches that reveal all cavities in a protein,[13,14] the TLES method exposes only tunnels accessible from a preselected initial ligand position. Applying this approach, we mapped a network of O_2 diffusion tunnels in T leading from the distal heme sites to the solvent via multiple escape routes[12] that emanate mainly from O_2 docking sites within the tunnels. These sites in T[12] and in the isolated α-subunit[15] overlap the Xe cavities uncovered upon crystallization of HbA under Xe.[16] Similar cavities are found in myoglobin (Mb),[17] a monomeric globin structurally related to HbA. Overall, our computational analyses reveal that O_2 molecules placed in the distal heme pockets diffuse within the same well-

Received: July 22, 2014
Revised: July 2, 2015
Published: July 30, 2015

DOI: 10.1021/acs.biochem.5b00368
Biochemistry 2015, 54, 5268−5278

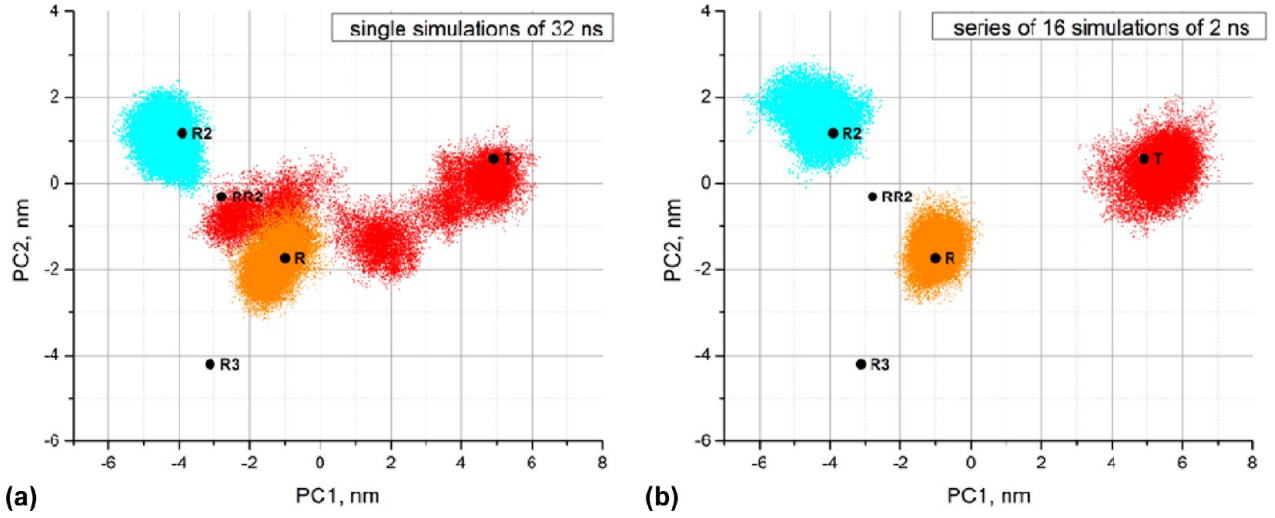

Figure 1. PCA projections of the simulated quaternary structures reveal that R and R2, but not T, remain close to their crystal structures over 32 ns simulations. The dots represent the PCA projections at 1 ps intervals onto the two motion components in Figure 2 starting from the T (red dots), R (orange dots), and R2 (cyan dots) tetrameric structures during (a) a single 32 ns simulation (which is representative of the three performed) and (b) 16 simulations 2 ns in duration with 15 unbound TLES O_2 copies in the α-subunits (which are representative of the 32 TLES simulations performed for each subunit and state). Note that the bound heme ligand was removed from R (PDB entry 2DN3) and R2 (PDB entry 1BBB) such that all simulations were performed with HbA in the unligated form. Black dots representing the RR2 (PDB entry 1MKO) and R3 (PDB entry 1YZI) crystal structures are shown for reference.

defined tunnels in all models. However, access to certain docking sites and escape routes is modified by subtle changes in subunit dynamics and heme movement linked to HbA's three quaternary states and by the conformation of the bulky indole side chain in the five tryptophan variants of HbA examined here.

COMPUTATIONAL PROCEDURES

Crystal structures of deoxyHbA and carbonmonoxyHbA were chosen as the initial structures for T [Protein Data Bank (PDB) entry 2DXM],[18] R (PDB entry 2DN3),[19] and R2 (PDB entry 1BBB).[6] The CO and distal water molecules were removed, and unligated O_2 molecules were placed in the α_1- or β_1-distal sites of the HbA tetramer at the site of bound O_2 in oxyHb. After structure equilibration, O_2 adopted positions approximately parallel to the heme plane, and all-atom MD simulations of O_2 diffusion were performed in explicit solvent at 310 K. Langevin dynamics with γ = 0.5 ps^{-1} and TLES[11] were combined for simulations of O_2 diffusion as implemented in NAMD version 2.7.[20] Thirty-two short (2 ns) simulations of the diffusion of 15 TLES O_2 were performed for each subunit and quaternary state.

The initial HbA variant structures chosen for the TLES simulations were T-state HbA(αH58W) (PDB entry 3NMM),[9] R-state HbA(βH63W) (PDB entry 3NL7),[9] T-state HbA-(αL29F,αH58Q,βV67W) (PDB entry 1O1M),[10] R-state HbA-(αL29F,αH58Q,βL106W) (PDB entry 1O1I),[10] and T-state HbA(αL29W) (PDB entry 1O1N).[10] Fifteen O_2 copies were placed in the β-distal sites of βTrpE11 (βW67) and βTrpG8 (βW106) and in the α-distal site of αTrpB10 (αW29) but in the αXe3 and αXe4 sites of αTrpE7 (αW58) because its α-distal site is occupied by the side chain of TrpE7. Sixteen replicate 2 ns simulations were performed for each starting position of the O_2 copies using the same procedures as for wild-type HbA.

Additionally, three ligand-free standard MD simulations of 32 ns were conducted for each of the wild-type T, R, and R2 forms. These long trajectories were used to analyze tertiary changes and polypeptide dynamics in the three states. Because T gradually undergoes the transition to RR2/R (Figure 1a), only the first 7.5 ns of these trajectories corresponding to the distinct T state was used in the analysis. The protein structures and the results were plotted using the VMD package[21] and Accelrys DS Visualizer.[22] Further details of system preparation and the simulation parameters are provided in the Supporting Information.

RESULTS

PCA Confirms HbA's Conformational Stability during Short Simulations. The HbA tetramer spontaneously undergoes quaternary transitions over typical MD simulation times of ~10−100 ns.[12,23] Because ligand migration in proteins occurs on similar time scales,[13,15,17] this complicates the use of standard MD to simulate gas diffusion within the crystallographyically defined HbA quaternary states. Starting from the T crystal structure, we demonstrated previously[12] that the HbA tetramer reliably represents the T quaternary and tertiary structure during the first 2−3 ns of the simulations. Thus, we combined all-atom MD simulations with the TLES approach[11] to accelerate ligand migration. Increasing the effective ligand temperature increases their intercavity transition rates without altering protein dynamics.[12,24,25] Moreover, the TLES method provides multiple diffusion trajectories per simulation by accommodating multiple noninteracting copies of the ligand that diffuse independently while the protein and water molecules experience an average ligand potential derived from all copies. Using a series of 2 ns TLES simulations, we found a tunnel network in T that is consistent with the results of standard MD simulations.[12,15,26]

From principal component analysis (PCA) of their C_α and heme atoms, de Groot and co-workers[23] reported that the quaternary structure of T, R, and R2 can be characterized by projections onto two principal components [PC1 and PC2 (Figure 2)]. The T → R transition involves linear motions

DOI: 10.1021/acs.biochem.5b00368
Biochemistry 2015, 54, 5268−5278

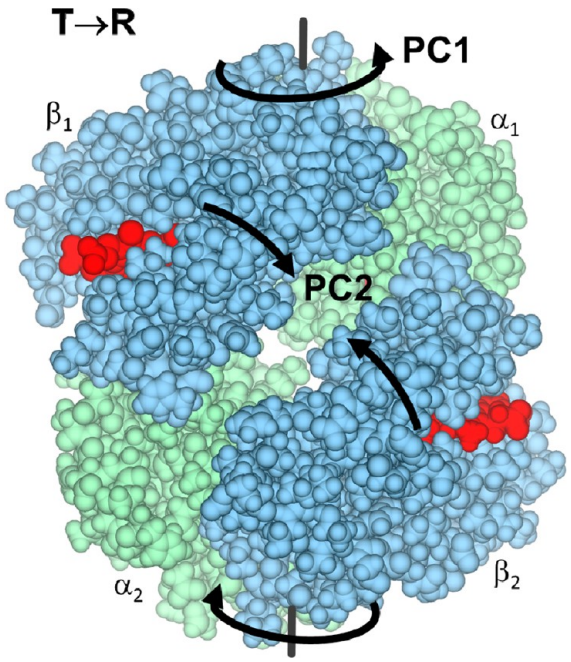

Figure 2. Two principal components characterize HbA's quaternary transitions. The crystal structure of T (PDB entry 2DXM) is shown with all atoms of the α-subunits (green), the β-subunits (blue), and the hemes (red) represented as spheres. PCA[23] of the C_α and heme atoms in the structures of T, R (PDB entry 2DN3), and R2 (PDB entry 1BBB) identified two motion components that describe the quaternary changes between these states. Linear motions along PC1 (89% variance) involve mainly large-scale rotation of the $\alpha_1\beta_1$ heterodimer relative to the $\alpha_2\beta_2$ heterodimer, whereas motions along PC2 (11% variance) alter the separation between the β-subunits.

mainly along PC1 (Figure 1), which correspond to rotation of the relatively rigid $\alpha_1\beta_1$ and $\alpha_2\beta_2$ heterodimers with respect to each other and results in significant changes at the heterodimer interfaces.[3] The R → R2 transition, on the other hand, involves equal motions along PC1 and PC2 (Figure 1), where PC2 tracks the approach of the β-subunits to each other (Figure 2). We performed standard MD simulations of the protein structures without ligands over 32 ns, and PCA projections of the structures reveal that both R and R2 sample conformations close to their crystal structures whereas T gradually undergoes the transition to RR2/R (Figure 1a), consistent with its documented low conformational stability.[12,23] In contrast, during multiple 2 ns trajectories, all states with TLES O_2 copies firmly represent their respective crystal subspaces (Figure 1b). Hence, we sampled O_2 trajectories within HbA only during short 2 ns simulations.

T, R, and R2 Possess the Same Diffusion Tunnel Profiles. The O_2 diffusion tunnels are lined mainly by hydrophobic residues [L, V, and A (Tables S1 and S2)] like in the monomeric globins.[14] Analogous to T,[12] ligands do not cross the subunit interfaces in R or R2; therefore, diffusion from the distal heme site in each subunit was considered independently, and 960000 ligand positions per subunit are plotted in Figure S1 for T, R, and R2. These positions define the diffusion pathways and escape portals (Table 1 and Table S3), while ligand density analysis uncovers docking sites separated by steric barriers (Figure 3 and Tables S1 and S2).[12] The diffusion tunnel profiles in T, R, and R2 are remarkably similar (Figure 3 and Figure S1). Collision frequencies confirm that the O_2 copies collide with the same residues in each state

Table 1. Use of Exit Portals Originating from the Most Densely Occupied Cavities in T, R, and R2

Portal[b]	Cavity	Helices and loops at portals	Portal usage (%)[a]		
			T	R	R2
1α 2α	αXe2	A, B, E AB, G	55	34	10
3α 4α	αXe3	CE, E, heme B, C, CE	22	30	32
6α	αXe6	A, H, GH	13	28	51
1β	βXe1	G, H	60	36	15
6β	β-distal	CD, E, heme	11	15	45

[a]The numbers indicate the percentages of TLES O_2 that use the indicated portals based on the total number of observed escapes (85–162) from the α- or β-subunit in 480 independent O_2 trajectories [$\sum\alpha$ and $\sum\beta$ all values (Table S3)]. Combined percentages are listed for portals 1α and 2α, as well as for portals 3α and 4α. [b]The bold red font distinguishes escape routes that lead directly to the solvent from the distal heme pockets from those that lead to the solvent via the interior α- or β-tunnels. Note that all escape portals are listed in Table S3.

(Figure 4), and these residues possess similar conformations based on crystal structure alignment (data not shown). As we reported previously for T,[12] the simulated O_2 docking sites in R and R2 overlap HbA's experimentally observed cavities for Xe[16] and photolyzed CO[27] (Figure 3).

The TLES O_2 copies placed in the α-distal site jiggle there for a short time before overcoming the αHisE7 or α-B10E11G8 steric barriers.[12] Many of the copies that enter the αXe3 site, which is connected directly to the solvent and highly populated (Figure S1a,c,e), return to the α-distal site, indicating that the protein's hydration shell imposes a significant barrier for escape of nonpolar O_2 to the aqueous solvent.[28] This increases the ligand dwell time within the protein matrix, allowing many O_2 copies to escape to the solvent from the long interior α-tunnel that encompasses five experimental Xe cavities (αXe1, -2, and -4–6) as well as a small cavity (termed a phantom site) near the αXe5 site (Figure 3a,c,e).

Notably, the TLES O_2 copies placed in the β-distal site promptly overcome the β-B10E11G8 barrier (analogous to the α-B10E11G8 barrier) and migrate to the wide β-tunnel, encompassing the βXe1, -1′, and -2 cavities (Figure 3b,d,f). The ligands spend most of their time jiggling in the β-tunnel except for brief visits to the β-distal heme site and a few phantom sites with poor ligand accessibility (Figure S1b,d,f). This contrasts with the O_2 motion in the α-subunit, where the ligands continuously hop between the more numerous and better delimited α-cavities. The fast ligand migration from the β-distal site to the β-tunnel, in which ligands readily accumulate, could explain the 3-fold slower geminate recombination in the β-subunit versus the α-subunit.[8,29]

O_2 Docking Site Occupancy and Escape Route Usage Vary among T, R, and R2. Table S3 lists all exit portals found in the simulations, and the most frequently used portals are summarized in Table 1. Although the diffusion tunnel topology does not change with quaternary structure, ligand densities in the docking sites and portal usage vary significantly among T, R, and R2 (Figure 5). Substantially more O_2 copies cross the α-G16H8A11 barrier to the αXe6 site in R and R2 than in T. Consequently, the largest variation in collision frequency

DOI: 10.1021/acs.biochem.5b00368
Biochemistry 2015, 54, 5268–5278

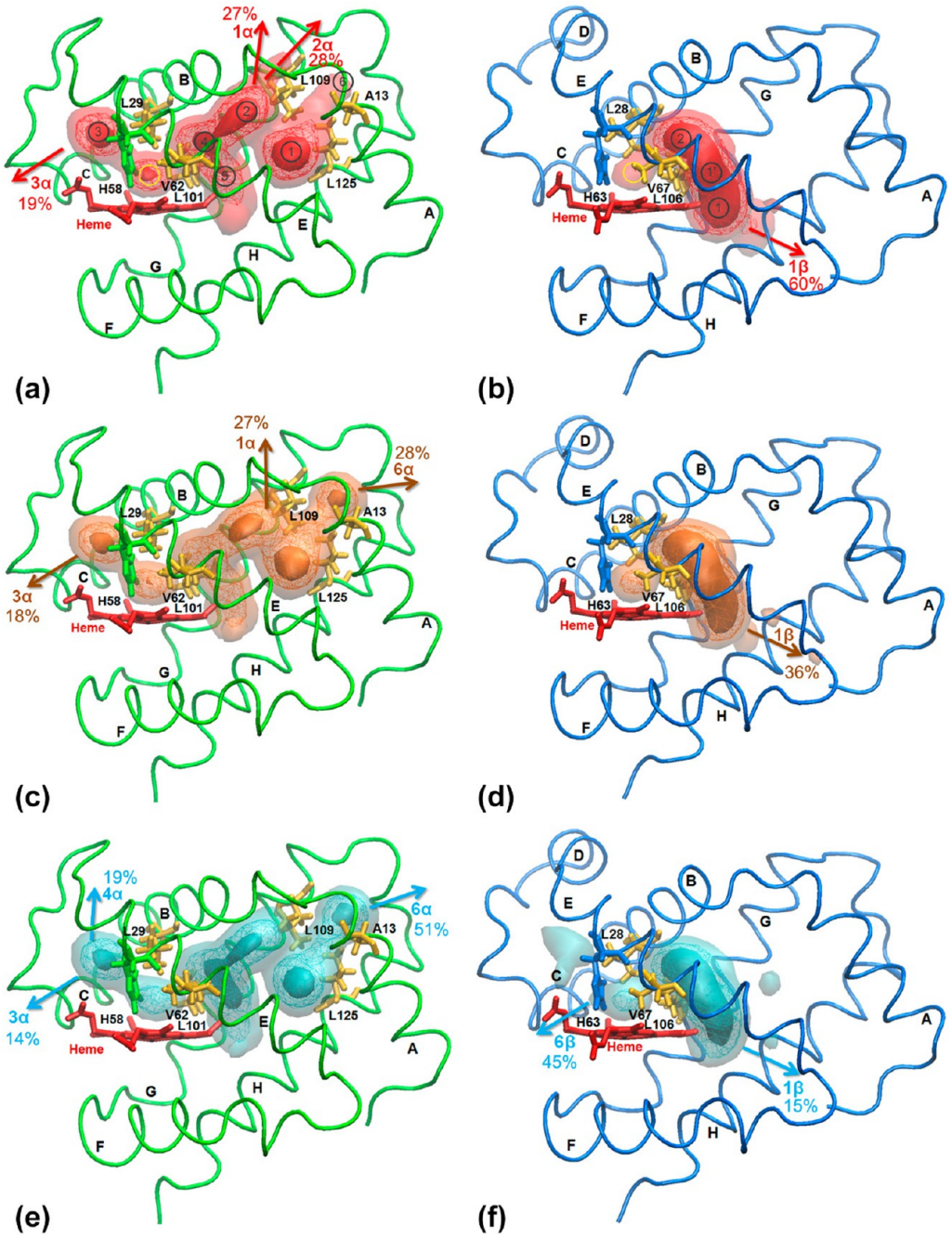

Figure 3. Comparison of O_2 distribution in the kinetically accessible diffusion tunnels in T, R, and R2. O_2 distribution maps of 480 trajectories with durations of 2 ns from TLES MD simulations of O_2 diffusing from the distal heme site of (a) the T α-subunit, (b) the T β-subunit, (c) the R α-subunit, (d) the R β-subunit, (e) the R2 α-subunit, and (f) the R2 β-subunit. Isosurfaces define regions with ≥0.375% (solid), ≥0.125% (wireframe), and ≥0.025% (transparent) average ligand occupancies during the simulations. Regions of high and low occupancy correspond to O_2 docking sites and barriers, respectively. Ribbons represent the backbone atoms of the α-subunits (green) and β-subunits (blue). The hemes (red), αHisE7 (green), βHisE7 (blue), α,β-B10E11G8 (amber), and α-G16H8A11 (amber) barriers are shown as sticks. The arrows indicate the frequently used exit portals, and the percentage of O_2 escapes via a given portal based on the total number of escapes (Table S3) is indicted. The positions in each subunit of 960000 O_2 molecules are shown in Figure S1, and the residues lining the tunnels are listed in Tables S1 and S2.

(Figure 4a) is with residues lining the αXe6 cavity [αA13, αL113, αE116, αF117, αV121, and αL125 (Table S1)]. Furthermore, a higher percentage of O_2 molecules escape via portal 6α in R2 (51%) and R (28%) than in T (13%) (Table 1). Reflecting the relative ligand occupancy of the αXe2 site (Figures 3a,c,e and 5a,c), 55 and 34% of escapes occur via combined portals 1α and 2α in T and R, respectively, but only 10% in R2 (Table 1). Consistent with our TLES results (Table 1), standard MD simulations on the isolated R α-subunit identified portals 1α, 4α, and 6α as major O_2 exits.[15] In the β-subunit, the low O_2 occupancy of the βXe1 site in R and R2 (Figures 3b,d,f and 5b,d) leads to an ∼2−4-fold drop in portal 1β usage in these states relative to that in T (Table 1). This promotes O_2 exodus via portal 6β in R2 (Table 1) but results in less O_2 escape overall from the R β-subunit [$\sum\beta$ all (Table S3)].

DOI: 10.1021/acs.biochem.5b00368
Biochemistry 2015, 54, 5268−5278

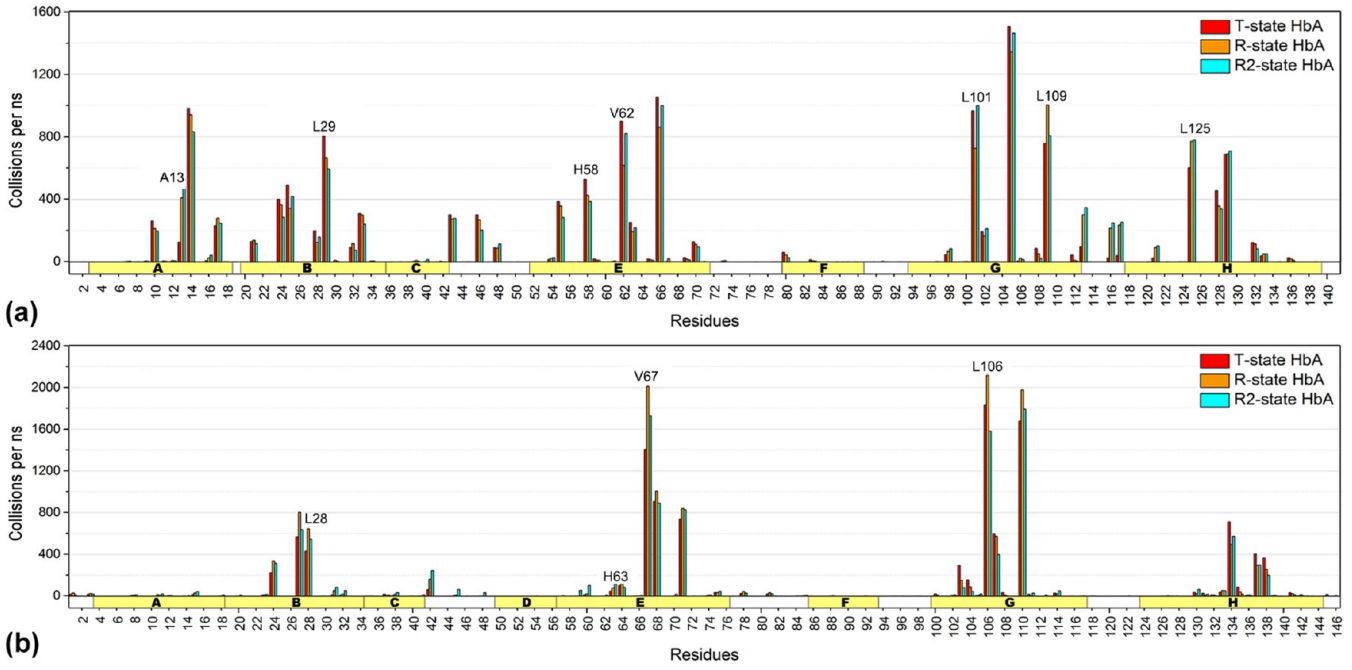

Figure 4. Maps of collision frequency between the O_2 copies and the residues in the T, R, and R2 quaternary states of HbA. Number of collisions per nanosecond with the atoms of a given residue summed over 480 trajectories of the TLES O_2 copies diffusing during 2 ns from the distal sites of the (a) α-subunit and (b) β-subunit of T, R, and R2. A collision is assumed to occur when an O_2 ligand and the closest residue atom are separated by ≤2.5 Å. These plots reveal that the same residues line the diffusion tunnels of T, R, and R2, but there are variations in collision frequencies. For example, the variation in collisions with αA13 and αL125 (a) reflects the O_2 populations in αXe6 (Figure 3a,c,e). Similarly, the variation in collision frequency at βV67 (b) reflects differential occupancy of the βXe2 and β-distal heme sites (Figure 3b,d,f). Helices A−H of both subunits are indicated by the yellow rectangles.

Quaternary-Linked Changes in Protein Dynamics Modulate O_2 Diffusion and Escape in the α-Subunit. Rotation of $\alpha_1\beta_1$ relative to $\alpha_2\beta_2$ (Figure 2) affects a number of close contacts and hydrogen bonds between these heterodimers.[3] The long αCE loop located near the heterodimer interface undergoes very large quaternary-linked mobility changes in the α-subunit, as reflected in the calculated *B* factors (Figure 6a and Figure S2a). Increased flexibility of this loop in R and R2 relative to T (Figure 6a) is transmitted to the heme pocket, but surprisingly, more O_2 copies accumulate in the less flexible T α-distal heme pocket, which comprises the αXe3 and α-distal sites (Figure 5a,c). Close examination of the heme region of the α-subunit during the simulations reveals a 0.1−0.2 Å heme translation and slight enlargement of the α-heme pocket in T, which counteracts the drop in flexibility and facilitates the access of O_2 to the T αFe. Thus, the dramatic changes in αCE loop flexibility (Figure S2a) are not accompanied by large differences in the percentage of O_2 escapes directly from the α-distal heme pocket in the three quaternary states (Table 1).

Although they are much less mobile than the αCE loop, quaternary-induced changes in the flexibility of the α-tunnel's AB and GH corners (Figure 6a and Figure S2a) have a more significant impact on O_2 diffusion. Increased flexibility at the AB corner increases the O_2 occupancy of αXe2 (Figure 5c) and hence the number of escapes via portals 1α and 2α in T versus R2 (Table 1). On the other hand, decreased flexibility at the GH corner disfavors migration of the ligands into αXe6 (Figure 5c) and escape through portal 6α falls in T versus R2 (Table 1). Overall, the preferred O_2 escape routes from the α-tunnel switch from portals 1α and 2α in T to portal 6α in R2, whereas a distinct portal preference is not seen for R because its αXe2 and αXe6 sites exhibit comparable O_2 occupancies (Figure 5a).

Quaternary-Linked Movement of the β-Heme Controls O_2 Diffusion and Escape in the β-Subunit. The truncated β-tunnel is surrounded by long rigid helices B, E, G, and H that exhibit similar dynamics in T, R, and R2 (Figure 6b and Figure S2b). However, the β-heme rotates and translates relative to helix E during the quaternary transitions. The volume of the β-distal heme site increases with the distance Δ_1 between the heme and the βHisE7 residue (Figure 7a), and quaternary-linked variation in the mean Δ_1 value reveals that the β-distal site is on average smaller in T than in R or R2 (Figure 7b,c). Hence, despite a more flexible βCD loop (Figure 6b and Figure S2b), increased steric hindrance between βHisE7 and incoming O_2 ligands reduces their access to the T βFe and decreases the T β-distal site O_2 population (Figures 3b,d,f and 5b,d).

β-Heme movement also is accompanied by a conformational change in residue βF71 lining the βXe1 site (Table S1). The quaternary-linked change in Δ_2, the separation between the β-heme and βF71, forces the phenyl ring to adopt an open conformation in T (Figure 8). This allows ligands to freely migrate between βXe1 and HbA's central water-filled cavity[12] as evidenced by the extensive use of portal 1β (Table 1) and the relatively high ligand density in the central cavity in T (Figure 3b). βF71 switches to its closed conformation with the phenyl ring partially capping the βXe1 site in R and R2 (Figure 8a), which restricts diffusion of the ligand into the central cavity via portal 1β (Figure 5b,d and Table 1). Hence, by controlling the size of the β-distal heme and βXe1 sites, quaternary-linked movement of the β-heme drives ligand redistribution in the β-

DOI: 10.1021/acs.biochem.5b00368
Biochemistry 2015, 54, 5268−5278

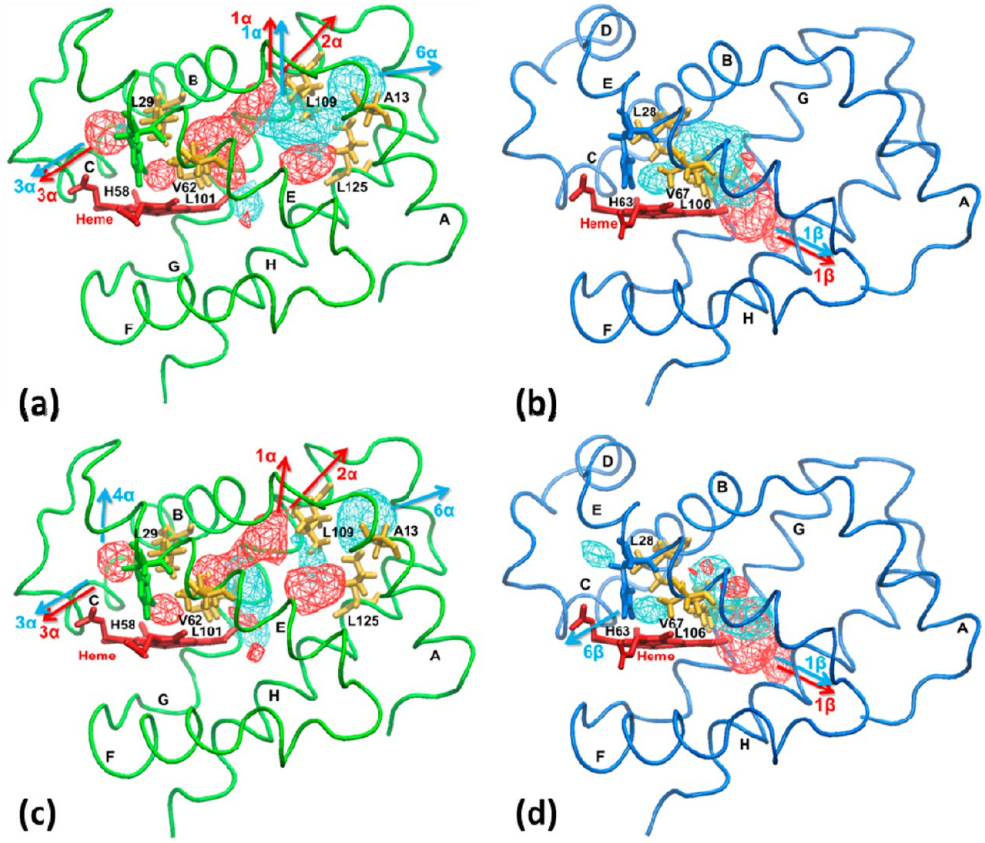

Figure 5. Differences in O_2 distribution in the kinetically accessible diffusion tunnels in T vs R and R2. (a and b) T−R and (c and d) T−R2 difference maps of the O_2 distribution in the α-subunits (left) and β-subunits (right). Isosurfaces in the difference maps are based on the O_2 distributions shown in Figure 3 and delineate the contour at three standard deviations in the O_2 occupancies, with the red and blue isosurfaces corresponding to larger O_2 populations in T and R/R2, respectively. For example, in panel c, the red isosurfaces reveal a larger O_2 population in the αXe1, αXe2, αXe3, and α-distal sites in T vs R2, whereas the blue isosurfaces uncover a larger O_2 population in αXe5 and αXe6 in R2 vs T. Ribbons represent the backbone atoms of the α-subunits (green) and β-subunits (blue). The hemes (red), HisE7 barriers [distal histidines αH58 (green) and βH63 (blue)], B10E11G8 barriers (residues αL29, αV62, and αL101 or βL28, βV67, and βL106), and α-barrier G16H8A11 (residues αL109, αL125, and α13) (amber) are shown as sticks. The arrows denote the frequently used exit portals in T (red) and R or R2 (blue) (Table 1).

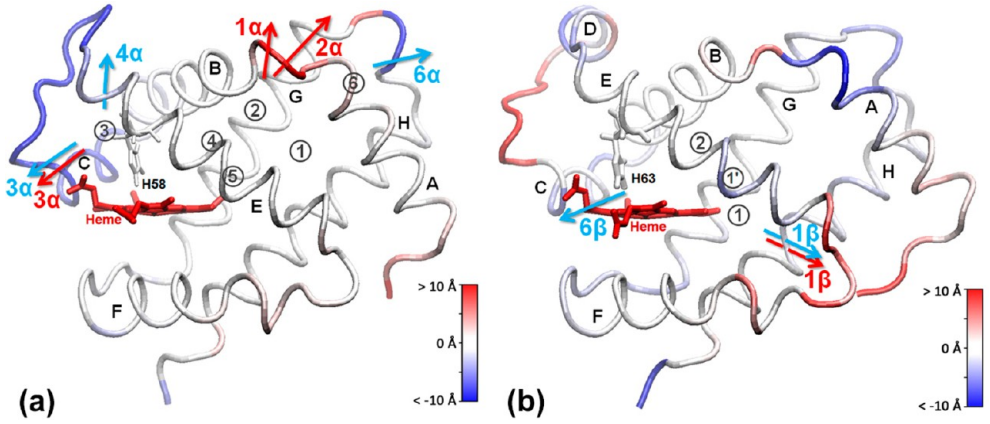

Figure 6. Changes in subunit mobility between T and R2 are located at the αCE and βCD loops, and the αAB and αGH corners. The backbone atoms of the (a) T α-subunits and (b) T β-subunits (ribbons) are colored according to the *B* factor differences (in angstroms) between the Cα atoms in T and R2, which are plotted in Figure S2. The red and blue regions of the chains are more mobile in T and R2, respectively. The hemes are represented as red sticks, and the black circles denote the experimental Xe docking sites.[16] The red and blue arrows identify the frequently used exit portals in T and R2, respectively.

subunit, leading to the preferred use of portal 1β in T compared to portal 6β in R2 (Table 1).

Tryptophan Substitution in the Distal Pockets Restricts or Prevents Access to Selected Cavities. We simulated O_2 diffusion in five structurally characterized HbA variants with tryptophan substitutions in the distal heme pockets.[9,10] The crystal structure of the T αTrpE7 variant reveals that the mutated E7 residue adopts a closed

DOI: 10.1021/acs.biochem.5b00368
Biochemistry 2015, 54, 5268−5278

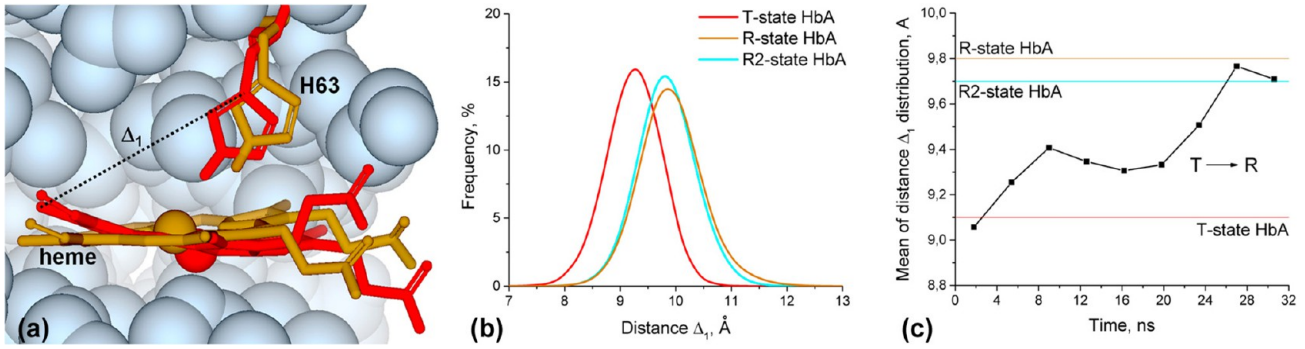

Figure 7. Separation between the heme and residue βHisE7 (H63) increases during the T → R transition. (a) Superimposed crystal structures of the T and R β-subunits showing the distance Δ_1 between the C_γ atom of βH63 and the C_{MC} atom of the heme. The blue spheres represent the protein atoms of the T β-subunit, and the heme and βH63 are depicted as red and brown sticks in T and R, respectively. During the T → R transition, the β-heme rotates by 25° around its N_B–N_D bond and moves away from helix E by 0.7 Å. (b) Distributions of the Δ_1 values measured during 32 ns ligand-free simulations of the distinct T, R, and R2 states. (c) Changes in the mean Δ_1 values during the simulated T → R transition plotted at 3.5 ns intervals. At 0–3.5 ns, the mean Δ_1 corresponds to that of T and approaches that of the overlapping R and R2 distributions at 25–32 ns.

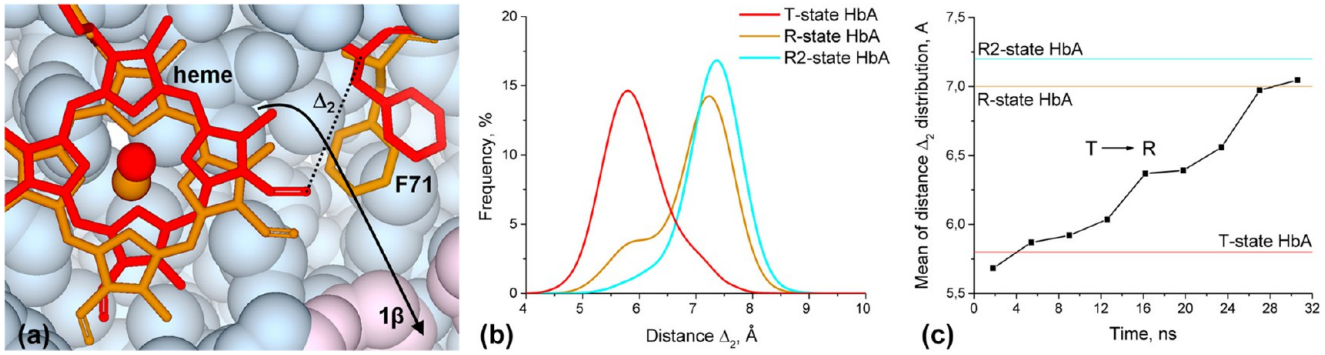

Figure 8. Separation between the heme and residue βF71 (F71) increases during the T → R transition. (a) Superimposed crystal structures of T and R showing the distance Δ_2 between the C_α atom of residue βF71 and the C_{BB} atom of the heme vinyl group. The heme and βF71 are depicted as red and brown sticks in T and R, respectively. The blue spheres represent the protein atoms of the T β-subunit except for those lining portal 1β, which are represented by pink spheres. (b) Distributions of the Δ_2 values measured during ligand-free simulations of distinct T, R, and R2. (c) Changes in the mean Δ_2 values during the simulated T → R transition plotted at 3.5 ns intervals. At 0–3.5 ns, the mean Δ_2 corresponds to that of T and approaches that of the overlapping R and R2 distributions at 25–32 ns.

conformation with the bulky indole ring anchored in the α-B10E11G8 barrier.[9] This fully blocks access of the ligand to the α-distal heme cavity; therefore, O_2 copies initially placed in the αXe3 site quickly escape to the solvent mainly via portal 3α, while those placed in αXe4 exit the α-tunnel via multiple portals (Figure 9a and Table S4). In contrast, β-heme access is increased in the R βTrpE7 variant (Figure 9b) because the indole group extends out to the solvent unlike the smaller native imidazole group.[9] The indole ring remains in this open conformation during the simulations and rotates around the side chain C_β–C_γ and C_α–C_β bonds to avoid clashing with the heme. Enlargement of the β-heme pocket in this variant boosts its O_2 occupancy (Figure 9b vs Figure 3d), allowing 3.5-fold more O_2 to directly escape from the β-distal heme in R βTrpE7 than in wild-type R (Tables S3 and S4).

Access to the β-tunnel via barrier β-B10E11G8 is prevented in the T βTrpE11 variant bearing the ValE11Trp mutation[10] (Figure 9c). This compels the O_2 copies to quickly escape from the small β-distal pocket to the solvent via the closest exit [portal 6β (Figure 9c and Table S4)] instead of accumulating in the large β-tunnel as in wild-type T (Figure 3b and Table S3). In the R βTrpG8 variant,[10] the indole group occupies the βXe1 site and blocks exit 1β, driving O_2 redistribution within the β-tunnel (Figure 9d and Table S4) and promoting escape via routes that are rarely used in the wild-type R β-subunit (Figure 3d and Table S3). In the T αTrpB10 variant,[10] the side chain of TrpB10 partially occupies the α-distal site, promoting diffusion of the ligand to the αXe3 site, which increases its ligand density compared to that in the wild-type T α-subunit (Figure 9e vs Figure 3a). No return to the α-distal site is observed during the simulations with HisE7 closed, and ligands escape mainly via portal 3α and less frequenctly via the α-front portal (Figure 9e and Table S4). Also, O_2 rarely diffuses to the interior tunnel of this variant.

DISCUSSION

Our MD simulations of O_2 diffusion in the HbA tetramer show that T, R, and R2 possess the same gas diffusion tunnels (Figure 3 and Figure S1) and patterns of ligand movement within these tunnels (Figure 4). These results are consistent with the experimental observation that quaternary states do not influence rates of association of NO to Hb.[30] Because binding of NO to the heme iron is limited by its diffusion through the protein,[30] the lack of dependence on the quaternary state suggests similar ligand motions in T and R. However, we also pinpoint changes in α-chain dynamics and β-heme position that couple docking site occupancy and portal use within the tunnels to the quaternary structure of the HbA tetramer. A total of 19 unique O_2 exit portals are identified (Table S3), which

DOI: 10.1021/acs.biochem.5b00368
Biochemistry 2015, 54, 5268–5278

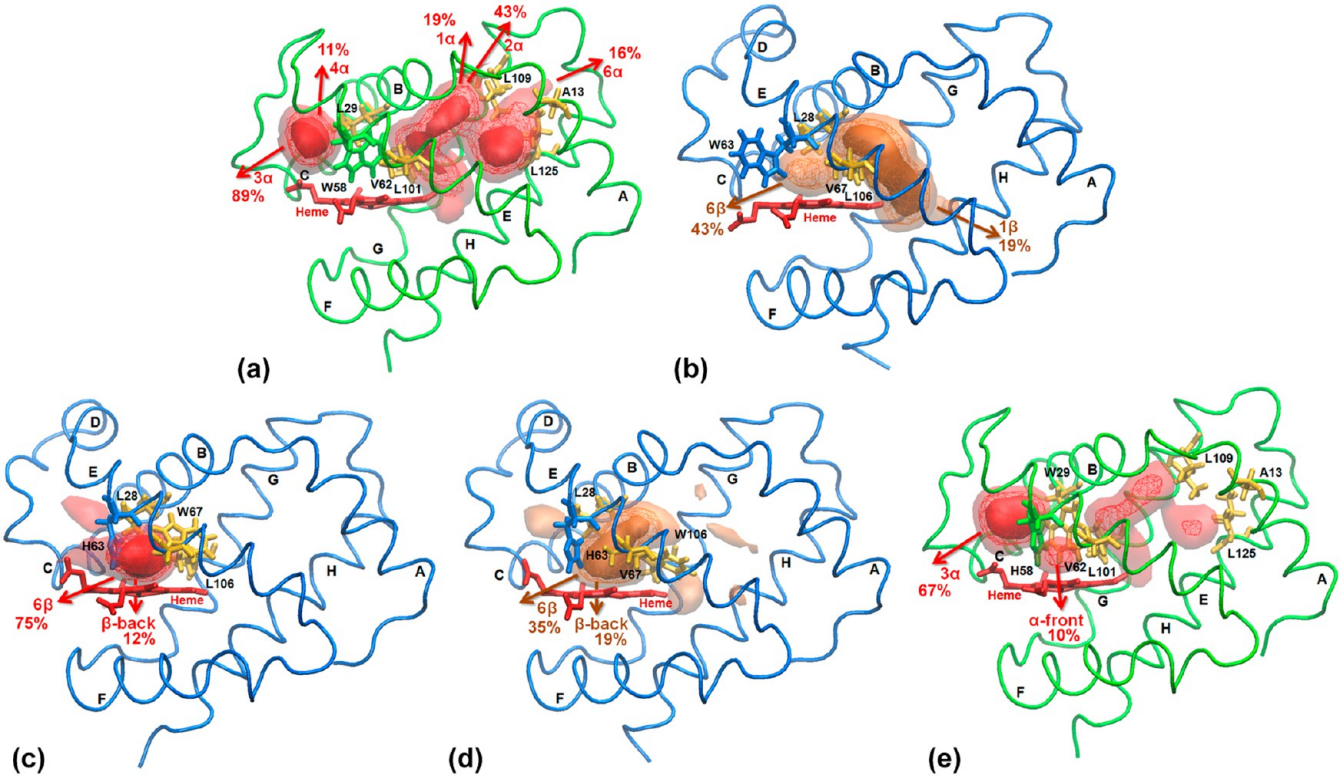

Figure 9. Trp substitution in the distal heme pockets alters the kinetically accessible diffusion tunnels in HbA. The O_2 distribution maps were plotted using 240 trajectories 2 ns in duration of TLES O_2 diffusing from (a) the αXe3 or αXe4 sites of the T αTrpE7 (H58W) variant, and from the β-distal heme site of the (b) R βTrpE7 (H63W), (c) T βTrpE11 (V67W), (d) R βTrpG8 (L106W) variants, and (e) from the α-distal site of the T αTrpB10 (L29W) variant. Isosurfaces define regions with ≥0.375% (solid), ≥0.125% (wireframe), and ≥0.025% (transparent) average occupancies during the simulations. Ribbons represent the backbone atoms of the α-subunits (green) and β-subunits (blue). The hemes (red), αHisE7 (green), βHisE7 (blue), α,β-B10E11G8 (amber), and α-G16H8A11 (amber) barriers are shown as sticks. The arrows denote the frequently used exit portals, and the percentage of O_2 escapes via a given portal based on the total number of escapes (Table S4) is indicated.

demonstrates the high porosity of HbA to small apolar gases like many of the monomeric globins, including Mb.[14,17,31,32] A subset of seven portals is used predominantly in HbA, with each quaternary state favoring two or three portals from this subset (Table 1).

From the data in Table S3, we calculate an average of 77, 69, and 54% of O_2 escapes from the interior α- plus β-tunnels in T, R, and R2, respectively. Recent MD simulations of T in an O_2-rich water environment revealed that O_2 also enters HbA via multiple routes[26] that coincide with the exit routes reported here. In fact, 73% of O_2 molecules enter HbA through the α- and β-tunnels, which is close to our estimate of 77% of O_2 escapes from these tunnels in T (Table S3). In Mb, ∼50% of ligand escapes occur from the interior tunnels and ligands also enter through multiple routes.[13] In summary, atomistic simulations of diffusion demonstrate that ligands reside in several interior cavities in HbA and Mb and exit and enter these cavities via numerous portals.

Recently, a picosecond Laue crystallographic study revealed biphasic CO geminate recombination in the R β-subunit, indicating the presence of at least two docking sites in this subunit.[33] The faster phase likely corresponds to recombination from the β-distal heme site, and the slower phase probably involves recombination of ligands that had diffused to the β-tunnel (Figure 3b,d,f). The authors[33] additionally associated the slower CO geminate rebinding phase with the existence of interior docking sites in the α-subunit. Multiphasic geminate recombination was also reported in picosecond time-resolved studies of oxyHbA,[34,35] which supports diffusion of O_2 into a number of regions of the protein. Furthermore, a cryogenic X-ray crystallographic study demonstrates experimentally that photolyzed CO ligands rapidly enter the β-tunnel of hybrid T-state carbonmonoxyHbA,[27] consistent with our observation that O_2 molecules placed in the β-distal heme sites promptly diffuse into the β-tunnel. Similarly, migration of the ligand from Mb's distal heme site to its interior tunnel network has been established by numerous cryogenic and time-resolved X-ray crystallographic studies[17,36−42] as well as MD simulations.[13,14,43−45]

Both experiment and simulation support diffusion of the ligands between the distal heme sites and the interior cavities of HbA and Mb. Furthermore, our simulations reveal that many of the O_2 molecules that diffuse into the α- and β-tunnels of HbA actually escape to the solvent from these tunnels (Table S3). However, it has been proposed from experimental results that although ligands may visit the interior tunnels, they mostly escape to the solvent from the heme pockets.[8,10,32,33,46] For example, an insignificant change in ligand kinetics upon mutation of residues in the interior tunnels is cited as evidence that ligands do not exit through these tunnels,[32,46] but as discussed below, alternative exit routes may compensate for blockage of a specific route upon mutation of a highly porous protein such as HbA. Ligand escape via multiple portals is difficult to confirm or refute experimentally.[17,32,47] Nonetheless, the increased electron density and residue movement detected on repeated pulsed laser illumination at cryogenic temperatures

DOI: 10.1021/acs.biochem.5b00368
Biochemistry 2015, 54, 5268−5278

around cavity Xe3 located 15 Å from the heme can be viewed as experimental evidence of CO escape via Mb's interior tunnels.[37]

Quaternary-Linked Variation in O_2 Escape Routes from the α-Subunit Is Evident for T, R, and R2. Our simulations predict similar O_2 escape rates from the α-subunits in the three quaternary states [$\sum\alpha$ all values (Table S3)]. Nonetheless, there is a clear preference for escape from αXe2 via portals 1α and 2α in T and from αXe6 via portal 6α in R2 (Table 1). We find that less O_2 exits via portal 6α and the phantom sites than enters via these routes, but this may reflect the computational instability of T (Figure 1)[12,23] during the previously reported 8 ns simulations of O_2 entry.[26] Despite the intrinsically greater accessibility of the T versus the R or R2 αFe (Figure 5a,c), ligand reactivity in T is attenuated by factors other than protein steric hindrance. High tension in helix F and other proximal constraints in the T α-subunit, as well as a distal water,[26,48] impose additional barriers to binding of the ligand to the T α-heme.[27,49,50]

More than 40 years ago, Perutz first described structural differences between the α- and β-distal heme sites of HbA. The relative O_2 populations in panels a and b of Figure 3 uphold the proposal by Perutz that ligands should be better accommodated in the α-distal site than in the β-distal site. This is supported experimentally by slower ligand escape upon photolysis from the α-site[27,33] as well as its higher level of hydration[19,50] compared to that of the β-distal site.

Quaternary-Linked Variation in O_2 Escape Routes from the β-Subunit Is Evident for T, R, and R2. Steric hindrance gives rise to the low O_2 occupancy of the T β-distal site (Figure 3b). This, combined with unhindered diffusion of O_2 through portal 1β into HbA's large central cavity, facilitates escape of O_2 from the T β-tunnel (Table 1). We count only escapes to the bulk solvent in Table S3 but note that O_2 rapidly diffuses between the β-tunnel and the central cavity in T with residue βF71 in its open conformation (Figure 8). Movement of the β-heme during the T → R transition (Figure 7) reduces steric hindrance in the β-distal site, thereby increasing ligand accessibility to the βFe in R and R2 versus T (Figure 5b,d). The T → R transition also induces partial closure of portal 1β as residue βF71 switches to its closed conformation (Figure 8), and HbA's central cavity is more compact and shielded from the bulk solvent in R and R2 than in T.[3−5] Nonetheless, as in the α-subunit, we find similar numbers of O_2 escapes from the T and R2 β-subunits [$\sum\beta$ all values (Table S3)], but the dominant portal switches from 1β in the β-tunnel in T to portal 6β leading from the β-distal heme site in R2 (Table 1). Conspicuously, the number of escapes from the R β-subunit is close to half that found for the T and R2 β-subunits [$\sum\beta$ all values (Table S3)]. The 1β portal remains the main exit from the R β-subunit, but partial blockage of this portal by residue βF71 (Figure 8) is not offset by increased direct escape from the distal heme pocket as seen for R2 (Table 1 and Table S3). Finally, we note that the quaternary-linked sliding of the β-heme exposed by our simulations is clearly observed experimentally on photolysis of hybrid T-state carbonmonoxyHbA crystals at cryogenic temperatures.[27]

Mutation-Linked Changes in O_2 Densities Are Consistent with the Experimental Gas Binding Kinetics of the Heme Pocket Variants. Several studies have investigated ligand diffusion in heme pocket variants of HbA, including those with HisE7 mutated to a bulky tryptophan.[8−10] Laser photolysis reveals multiphasic bimolecular rebinding of CO to the hemes of the isolated HbA subunits of the HisE7Trp variants, which is attributed to multiple conformations of TrpE7.[8,9] In the T αTrpE7 variant, for example, the indole ring in its closed conformation prevents heme access either directly from the solvent or from the α-tunnel (Figure 9a). Hence, the slow kinetic phase associated with indole reorientation[9] involves recombination with the heme of the photolyzed CO molecules that enter the distal site either directly from the solvent or via the α-tunnel. In fact, the latter may dominate because simulated entry of O_2 into T occurs mainly via its interior tunnels.[26] Our simulations demonstrate that no escape routes from the distal heme pocket are blocked in the R βTrpE7 variant and the increased experimental ligand escape rate in this variant[8] is consistent with efficient diffusion of O_2 through its distal portal 6β (Figure 9b).

The experimental rate of escape to the solvent also increases when access to the β-tunnel is blocked by the βValE11Trp mutation in the β-B10E11G8 barrier.[10] In agreement, the simulations show that O_2 copies placed in the small β-distal pocket of the T βTrpE11 variant quickly escape to the solvent via the closest portal, 6β (Figure 9c). Blocking β-tunnel access also dramatically increases the fraction of rapid geminate recombination to the heme after photolysis[10] because the photolyzed ligands are prevented from promptly diffusing to the β-tunnel as observed by cryogenic X-ray crystallography for wild-type HbA.[27] The fraction of slow geminate recombination decreases to ∼0 in the T αTrpB10 varaint[10] where the large indole group introduced into the α-B10E11G8 barrier partially occupies the α-distal site. Our simulations reveal that this inhibits the accumulation of the ligand in this site and promotes escape of the ligand to the neighboring cavities and to the solvent (Figure 9e).

The βLeuG8Trp mutation in the β-B10E11G8 barrier, on the other hand, leads to insignificant changes in the geminate ligand rebinding kinetics in the R βTrpG8 variant.[10] Presumably, portal 1β blockage by the large indole ring is offset by enhanced CO escape via portals leading from the minor cavities occupied in this variant (Figure 9d). Similar small changes in kinetics were observed upon substitution of residues in Mb's internal tunnels.[46] Also, in wild-type HbA, experimental CO−heme recombination rates did not significantly change under high Xe pressure, which was viewed as evidence that photolyzed CO directly escapes to the solvent without diffusing into any Xe cavities (Figure 3).[10] However, we previously demonstrated that a Xe atom placed in the interior tunnels diffuses between its multiple binding sites and does not perturb O_2 migration in T.[12] Given that the three quaternary states possess the same diffusion tunnels, we anticipate that added Xe would also have no effect on O_2 diffusion in R and R2, consistent with the absence of an experimental kinetic effect.[10]

■ CONCLUSIONS

Our simulations demonstrate at the atomic level that HbA's gas diffusion tunnels are the same in T, R, and R2. Subtle quaternary-linked changes in α-subunit dynamics and β-heme position trigger the redistribution of O_2 among its numerous docking sites within the tunnels, which results in a dramatic change in portal use upon the transition from T to R2 (Table 1). We speculate that the availability of many alternative gas exits linked to HbA's quaternary transitions is physiologically beneficial in the crowded environment of the red blood cell and could mitigate the consequences of point mutation in many

DOI: 10.1021/acs.biochem.5b00368
Biochemistry 2015, 54, 5268−5278

regions of the gas tunnels as seen for the βTrpG8 variants (Figure 9d). Also, because of HbA's high gas porosity, accompanying atomistic simulations of diffusion may contribute to the interpretation of changes in gas binding kinetics upon mutation or modification of the experimental conditions.

■ ASSOCIATED CONTENT

Supporting Information

The Supporting Information is available free of charge on the ACS Publications website at DOI: 10.1021/acs.biochem.5b00368.

Figures showing maps of O_2 positions within the kinetically accessible diffusion tunnels of T, R, and R2 and of the changes in flexibility of the polypeptide chains of R and R2 relative to T based on the calculated *B* factors, tables listing residues lining the cavities in the tunnel network of HbA, residues and barriers between neighboring cavities, and portal usage upon diffusion of O_2 from the distal heme sites in T, R, and R2 and the HbA variants, and supplemental experimental procedures (PDF)

■ AUTHOR INFORMATION

Corresponding Authors

*E-mail: gilles.peslherbe@concordia.ca. Telephone: 514-848-2424-3335. Fax: 514-848-2864.

*E-mail: ann.english@concordia.ca. Telephone: 514-848-2424-3338. Fax: 514-848-2864.

Funding

This work was funded by FRQ-NT (Quebec) and NSERC (Canada). M.S.S. is the recipient of a PROTEO postdoctoral fellowship (FRQ-NT), and G.H.P. is a Concordia University Research Fellow.

Notes

The authors declare no competing financial interest.

■ ACKNOWLEDGMENTS

Computational resources were provided by Calcul Québec, Compute Canada, and the Centre for Research in Molecular Modeling (CERMM).

■ ABBREVIATIONS

HbA, human hemoglobin; R, relaxed quaternary state; T, tense quaternary state; Mb, myoglobin; MD, molecular dynamics; TLES, temperature-controlled locally enhanced sampling.

■ REFERENCES

(1) Perutz, M. F. (1989) Mechanisms of cooperativity and allosteric regulation in proteins. *Q. Rev. Biophys. 22*, 139−237.

(2) Perutz, M. F. (1970) Stereochemistry of cooperative effects in haemoglobin. *Nature 228*, 726−739.

(3) Lukin, J. A., and Ho, C. (2004) The structure-function relationship of hemoglobin in solution at atomic resolution. *Chem. Rev. 104*, 1219−1230.

(4) Safo, M. K., and Abraham, D. J. (2005) The enigma of the liganded hemoglobin end state: a novel quaternary structure of human carbonmonoxy hemoglobin. *Biochemistry 44*, 8347−8359.

(5) Yuan, Y., Tam, M. F., Simplaceanu, V., and Ho, C. (2015) New Look at Hemoglobin Allostery. *Chem. Rev. 115*, 1702−1724.

(6) Silva, M. M., Rogers, P. H., and Arnone, A. (1992) A third quaternary structure of human hemoglobin A at 1.7-A resolution. *J. Biol. Chem. 267*, 17248−17256.

(7) Smith, F. R., and Simmons, K. C. (1994) Cyanomet human hemoglobin crystallized under physiological conditions exhibits the Y quaternary structure. *Proteins: Struct., Funct., Genet. 18*, 295−300.

(8) Birukou, I., Schweers, R. L., and Olson, J. S. (2010) Distal histidine stabilizes bound O_2 and acts as a gate for ligand entry in both subunits of adult human hemoglobin. *J. Biol. Chem. 285*, 8840−8854.

(9) Birukou, I., Soman, J., and Olson, J. S. (2011) Blocking the gate to ligand entry in human hemoglobin. *J. Biol. Chem. 286*, 10515−10529.

(10) Birukou, I., Maillett, D. H., Birukova, A., and Olson, J. S. (2011) Modulating distal cavities in the alpha and beta subunits of human HbA reveals the primary ligand migration pathway. *Biochemistry 50*, 7361−7374.

(11) Cohen, J., Kim, K., King, P., Seibert, M., and Schulten, K. (2005) Finding gas diffusion pathways in proteins: application to O_2 and H_2 transport in CpI [FeFe]-hydrogenase and the role of packing defects. *Structure 13*, 1321−1329.

(12) Shadrina, M. S., English, A. M., and Peslherbe, G. H. (2012) Effective Simulations of Gas Diffusion Through Kinetically Accessible Tunnels in Multisubunit Proteins: O_2 Pathways and Escape Routes in T-state Deoxyhemoglobin. *J. Am. Chem. Soc. 134*, 11177−11184.

(13) Ruscio, J. Z., Kumar, D., Shukla, M., Prisant, M. G., Murali, T. M., and Onufriev, A. V. (2008) Atomic level computational identification of ligand migration pathways between solvent and binding site in myoglobin. *Proc. Natl. Acad. Sci. U. S. A. 105*, 9204−9209.

(14) Cohen, J., and Schulten, K. (2007) O_2 migration pathways are not conserved across proteins of a similar fold. *Biophys. J. 93*, 3591−3600.

(15) Lepeshkevich, S. V., Biziuk, S. A., Lemeza, A. M., and Dzhagarov, B. M. (2011) The kinetics of molecular oxygen migration in the isolated alpha chains of human hemoglobin as revealed by molecular dynamics simulations and laser kinetic spectroscopy. *Biochim. Biophys. Acta, Proteins Proteomics 1814*, 1279−1288.

(16) Savino, C., Miele, A. E., Draghi, F., Johnson, K. A., Sciara, G., Brunori, M., and Vallone, B. (2009) Pattern of cavities in globins: the case of human hemoglobin. *Biopolymers 91*, 1097−1107.

(17) Tomita, A., Kreutzer, U., Adachi, S., Koshihara, S. Y., and Jue, T. (2010) 'It's hollow': the function of pores within myoglobin. *J. Exp. Biol. 213*, 2748−2754.

(18) Chatake, T., Shibayama, N., Park, S. Y., Kurihara, K., Tamada, T., Tanaka, I., Niimura, N., Kuroki, R., and Morimoto, Y. (2007) Protonation states of buried histidine residues in human deoxyhemoglobin revealed by neutron crystallography. *J. Am. Chem. Soc. 129*, 14840−14841.

(19) Park, S. Y., Yokoyama, T., Shibayama, N., Shiro, Y., and Tame, J. R. (2006) 1.25 A resolution crystal structures of human haemoglobin in the oxy, deoxy and carbonmonoxy forms. *J. Mol. Biol. 360*, 690−701.

(20) Phillips, J. C., Braun, R., Wang, W., Gumbart, J., Tajkhorshid, E., Villa, E., Chipot, C., Skeel, R. D., Kale, L., and Schulten, K. (2005) Scalable molecular dynamics with NAMD. *J. Comput. Chem. 26*, 1781−1802.

(21) Humphrey, W., Dalke, A., and Schulten, K. (1996) VMD: visual molecular dynamics. *J. Mol. Graphics 14*, 33−38.

(22) *D.S.M.E.*, release 3.5 (2012) Accelrys Software Inc., San Diego.

(23) Hub, J. S., Kubitzki, M. B., and de Groot, B. L. (2010) Spontaneous quaternary and tertiary T-R transitions of human hemoglobin in molecular dynamics simulation. *PLoS Comput. Biol. 6*, e1000774.

(24) Czerminski, R., and Elber, R. (1991) Computational studies of ligand diffusion in globins: I. Leghemoglobin. *Proteins: Struct., Funct., Genet. 10*, 70−80.

(25) Das, B., Helms, V., Lounnas, V., and Wade, R. C. (2000) Multicopy molecular dynamics simulations suggest how to reconcile crystallographic and product formation data for camphor enantiomers bound to cytochrome P-450cam. *J. Inorg. Biochem. 81*, 121−131.

(26) Takayanagi, M., Kurisaki, I., and Nagaoka, M. (2013) Oxygen entry through multiple pathways in T-state human hemoglobin. *J. Phys. Chem. B 117*, 6082−6091.

DOI: 10.1021/acs.biochem.5b00368
Biochemistry 2015, 54, 5268−5278

(27) Adachi, S., Park, S. Y., Tame, J. R., Shiro, Y., and Shibayama, N. (2003) Direct observation of photolysis-induced tertiary structural changes in hemoglobin. *Proc. Natl. Acad. Sci. U. S. A. 100*, 7039−7044.
(28) Austin, R. H., Beeson, K. W., Eisenstein, L., Frauenfelder, H., and Gunsalus, I. C. (1975) Dynamics of ligand binding to myoglobin. *Biochemistry 14*, 5355−5373.
(29) Olson, J. S., Rohlfs, R. J., and Gibson, Q. H. (1987) Ligand recombination to the alpha and beta subunits of human hemoglobin. *J. Biol. Chem. 262*, 12930−12938.
(30) Kim-Shapiro, D. B. (2004) Hemoglobin-nitric oxide cooperativity: is NO the third respiratory ligand? *Free Radical Biol. Med. 36*, 402−412.
(31) Elber, R. (2010) Ligand diffusion in globins: simulations versus experiment. *Curr. Opin. Struct. Biol. 20*, 162−167.
(32) Salter, M. D., Blouin, G. C., Soman, J., Singleton, E. W., Dewilde, S., Moens, L., Pesce, A., Nardini, M., Bolognesi, M., and Olson, J. S. (2012) Determination of ligand pathways in globins: apolar tunnels versus polar gates. *J. Biol. Chem. 287*, 33163−33178.
(33) Schotte, F., Cho, H. S., Soman, J., Wulff, M., Olson, J. S., and Anfinrud, P. A. (2013) Real-time tracking of CO migration and binding in the alpha and beta subunits of human hemoglobin via 150-ps time-resolved Laue crystallography. *Chem. Phys. 422*, 98−106.
(34) Lepeshkevich, S. V., Karpiuk, J., Sazanovich, I. V., and Dzhagarov, B. M. (2004) A kinetic description of dioxygen motion within alpha- and beta-subunits of human hemoglobin in the R-state: geminate and bimolecular stages of the oxygenation reaction. *Biochemistry 43*, 1675−1684.
(35) Lepeshkevich, S. V., Parkhats, M. V., Stepuro, II, and Dzhagarov, B. M. (2009) Molecular oxygen binding with alpha and beta subunits within the R quaternary state of human hemoglobin in solutions and porous sol-gel matrices. *Biochim. Biophys. Acta, Proteins Proteomics 1794*, 1823−1830.
(36) Chu, K., Vojtchovsky, J., McMahon, B. H., Sweet, R. M., Berendzen, J., and Schlichting, I. (2000) Structure of a ligand-binding intermediate in wild-type carbonmonoxy myoglobin. *Nature 403*, 921−923.
(37) Tomita, A., Sato, T., Ichiyanagi, K., Nozawa, S., Ichikawa, H., Chollet, M., Kawai, F., Park, S. Y., Tsuduki, T., Yamato, T., Koshihara, S. Y., and Adachi, S. (2009) Visualizing breathing motion of internal cavities in concert with ligand migration in myoglobin. *Proc. Natl. Acad. Sci. U. S. A. 106*, 2612−2616.
(38) Schmidt, M., Nienhaus, K., Pahl, R., Krasselt, A., Anderson, S., Parak, F., Nienhaus, G. U., and Srajer, V. (2005) Ligand migration pathway and protein dynamics in myoglobin: a time-resolved crystallographic study on L29W MbCO. *Proc. Natl. Acad. Sci. U. S. A. 102*, 11704−11709.
(39) Schotte, F., Lim, M., Jackson, T. A., Smirnov, A. V., Soman, J., Olson, J. S., Phillips, G. N., Jr., Wulff, M., and Anfinrud, P. A. (2003) Watching a protein as it functions with 150-ps time-resolved x-ray crystallography. *Science 300*, 1944−1947.
(40) Srajer, V., Teng, T., Ursby, T., Pradervand, C., Ren, Z., Adachi, S., Schildkamp, W., Bourgeois, D., Wulff, M., and Moffat, K. (1996) Photolysis of the carbon monoxide complex of myoglobin: nanosecond time-resolved crystallography. *Science 274*, 1726−1729.
(41) Srajer, V., Ren, Z., Teng, T. Y., Schmidt, M., Ursby, T., Bourgeois, D., Pradervand, C., Schildkamp, W., Wulff, M., and Moffat, K. (2001) Protein conformational relaxation and ligand migration in myoglobin: a nanosecond to millisecond molecular movie from time-resolved Laue X-ray diffraction. *Biochemistry 40*, 13802−13815.
(42) Hummer, G., Schotte, F., and Anfinrud, P. A. (2004) Unveiling functional protein motions with picosecond x-ray crystallography and molecular dynamics simulations. *Proc. Natl. Acad. Sci. U. S. A. 101*, 15330−15334.
(43) Cohen, J., Arkhipov, A., Braun, R., and Schulten, K. (2006) Imaging the migration pathways for O_2, CO, NO, and Xe inside myoglobin. *Biophys. J. 91*, 1844−1857.
(44) Maragliano, L., Cottone, G., Ciccotti, G., and Vanden-Eijnden, E. (2010) Mapping the network of pathways of CO diffusion in myoglobin. *J. Am. Chem. Soc. 132*, 1010−1017.
(45) Bossa, C., Anselmi, M., Roccatano, D., Amadei, A., Vallone, B., Brunori, M., and Di Nola, A. (2004) Extended molecular dynamics simulation of the carbon monoxide migration in sperm whale myoglobin. *Biophys. J. 86*, 3855−3862.
(46) Scott, E. E., Gibson, Q. H., and Olson, J. S. (2001) Mapping the pathways for O_2 entry into and exit from myoglobin. *J. Biol. Chem. 276*, 5177−5188.
(47) Huang, X., and Boxer, S. G. (1994) Discovery of new ligand binding pathways in myoglobin by random mutagenesis. *Nat. Struct. Biol. 1*, 226−229.
(48) Schotte, F., Soman, J., Olson, J. S., Wulff, M., and Anfinrud, P. A. (2004) Picosecond time-resolved X-ray crystallography: probing protein function in real time. *J. Struct. Biol. 147*, 235−246.
(49) Balakrishnan, G., Ibrahim, M., Mak, P. J., Hata, J., Kincaid, J. R., and Spiro, T. G. (2009) Linking conformation change to hemoglobin activation via chain-selective time-resolved resonance Raman spectroscopy of protoheme/mesoheme hybrids. *JBIC, J. Biol. Inorg. Chem. 14*, 741−750.
(50) Esquerra, R. M., Lopez-Pena, I., Tipgunlakant, P., Birukou, I., Nguyen, R. L., Soman, J., Olson, J. S., Kliger, D. S., and Goldbeck, R. A. (2010) Kinetic spectroscopy of heme hydration and ligand binding in myoglobin and isolated hemoglobin chains: an optical window into heme pocket water dynamics. *Phys. Chem. Chem. Phys. 12*, 10270−10278.

DOI: 10.1021/acs.biochem.5b00368
Biochemistry 2015, 54, 5268−5278